

## Accepted Manuscript

Water-resistant surfaces using zinc oxide structured nanorod arrays with switchable wetting property

Houda Ennaceri, Lan Wang, Darja Erfurt, Wiebke Riedel, Gauri Mangalgiri, Asmae Khaldoun, Abdallah El Kenz, Abdelilah Benyoussef, Ahmed Ennaoui

PII: S0257-8972(16)30316-4  
DOI: doi: [10.1016/j.surfcoat.2016.04.056](https://doi.org/10.1016/j.surfcoat.2016.04.056)  
Reference: SCT 21131

To appear in: *Surface & Coatings Technology*

Received date: 12 January 2016  
Revised date: 31 March 2016  
Accepted date: 24 April 2016



Please cite this article as: Houda Ennaceri, Lan Wang, Darja Erfurt, Wiebke Riedel, Gauri Mangalgiri, Asmae Khaldoun, Abdallah El Kenz, Abdelilah Benyoussef, Ahmed Ennaoui, Water-resistant surfaces using zinc oxide structured nanorod arrays with switchable wetting property, *Surface & Coatings Technology* (2016), doi: [10.1016/j.surfcoat.2016.04.056](https://doi.org/10.1016/j.surfcoat.2016.04.056)

This is a PDF file of an unedited manuscript that has been accepted for publication. As a service to our customers we are providing this early version of the manuscript. The manuscript will undergo copyediting, typesetting, and review of the resulting proof before it is published in its final form. Please note that during the production process errors may be discovered which could affect the content, and all legal disclaimers that apply to the journal pertain.

# Water-resistant surfaces using zinc oxide structured nanorod arrays with switchable wetting property

Houda Ennaceri<sup>(1,2)\*</sup>, Lan Wang<sup>3</sup>, Darja Erfurt<sup>4</sup>, Wiebke Riedel<sup>3,5</sup>, Gauri Mangalgi<sup>3</sup>, Asmae Khaldoun<sup>2</sup>, Abdallah El Kenz<sup>1</sup>, Abdelilah Benyoussef<sup>1</sup>, Ahmed Ennaoui<sup>(3,6,7)\*</sup>

<sup>1</sup>Laboratory of Magnetism and Physics of High Energies, URAC 12, Department of Physics, B.P. 1014, Faculty of Sciences, Mohammed V- Agdal University, Rabat, Morocco

<sup>2</sup>School of Science and Engineering, Al Akhawayn University, B.O. Box 104, Ifrane 53000, Morocco

<sup>3</sup>Helmholtz-Zentrum Berlin für Materialien und Energie, Hahn Meitner Platz 1, 14109 Berlin, Germany

<sup>4</sup>Technical University of Berlin (TU-Berlin), Straße des 17. Juni 135, 10632 Berlin, Germany

<sup>5</sup>Freie Universität Berlin, Takustr. 3, 14195 Berlin, Germany

<sup>6</sup>Qatar Environment and Energy Research Institute (QEERI), PO Box 5825, Doha, Qatar

<sup>7</sup>Hamad bin Khalifa University (HBKU), PO Box 5825, Doha, Qatar

\*E-mail Address: h.ennaceri@ui.ma  
aennaoui@qf.org.qa

## Abstract.

This study presents an experimental approach for fabricating super-hydrophobic coatings based on a dual roughness structure composed of zinc oxide nanorod arrays coated with a sputtered zinc oxide nano-layer. The ZnO nanorod arrays were grown by means of a low-temperature electrochemical deposition technique (75°C) on FTO substrates. The ZnO nanorods show a (002) orientation along the c-axis, and have a hexagonal structure, with an average length of 710 nm, and average width of 156 nm. On the other hand, the crystallite size of the top-coating sputtered ZnO layer is of 30 nm. The as-deposited ZnO nanorod arrays exhibited a hydrophobic behavior, with a surface water contact angle of 108°, whereas the dual-scale roughness ZnO nanorods coated with sputtered ZnO exhibited a super-hydrophobic behavior, with a surface water contact angle of 157° and a high water droplet adhesion. The photo-catalytic activity of the samples was investigated against the degradation of methylene blue under UV-A irradiation (365 nm). The ZnO nanorod arrays showed good photocatalytic activity whereas the superhydrophobic ZnO nanorod arrays top-coated with sputtered ZnO showed minimal activity regarding the degradation of methylene blue. The superhydrophobic films exhibited high sensitivity to UV light, with a UV-induced switching behavior from super-hydrophobic to super-hydrophilic after only 30 minutes of UV exposure.

**Key Words:** Super-hydrophobic, water contact angle, zinc oxide, nanorod arrays, rose petal effect, photo-catalysis.

### Highlights

- Hydrophobic ZnO nanorod arrays with high water-adhesion are achieved.
- Sputtered ZnO top-coating is used to reach super-hydrophobicity.
- Switchable wettability for ZnO single and dual roughness films under UV exposure.
- Strong pinning to the surface, similar to the rose-petal effect.
- The higher WCA is responsible for the decrease in the photo-catalysis activity.

## 1. Introduction and Background

Zinc oxide is an important n-type semiconducting material due to its wide band gap (3.37 eV at room temperature) [1] and large exciton binding energy (60 meV) [2]. ZnO is emerging as an efficient photo-catalyst due to its high surface reactivity, reaction and mineralization rates [3]. Because of the major importance of surface area and surface defects in the photo-catalytic activity of metal oxides, one dimensional structures such as nanowires or nanorods represent ideal candidate structures for photo-catalytic applications due to their large surface-to-volume ratio compared to thin films [4].

There is a big interest in growing ZnO nanorods for their potential use in different applications such as dye sensitized solar cells [5, 6], anti-reflective coatings (ARC) [7, 8, 9], light-emitting diodes [10], photo-catalysts [11-13], and gas sensing devices [14, 15]. Different processes have been reported to fabricate zinc oxide nanorods, such as physical vapor deposition [16, 17], chemical vapor deposition [18], wet chemical deposition [19, 20], ink-jet printing and hydrothermal processes [21, 22], surfactant assisted hydrothermal methods [23], vapor phase transport [24, 25], and pulsed laser deposition [26].

Electrochemical and chemical bath depositions conducted at low temperatures [27, 28] represent an easy, fast preparation and non-toxic process to prepare zinc oxide nanorod arrays. Moreover, they can be up-scaled for industrial applications.

Zinc oxide is intrinsically hydrophilic, which is due to the presence of hydroxyl groups on its surface [29, 30]. However, ZnO can be used to prepare hydrophobic surfaces by creating hierarchical structures and roughening the surfaces [31, 32]. There exist two types of super-hydrophobic surfaces, low and high water-adhesion super-hydrophobicity [33-35]. The first type is inspired from the lotus plant, and is observed with water contact angles exceeding  $150^\circ$ , and very low sliding angles (not exceeding  $10^\circ$ ) [36]. On the other hand, high water-adhesion super-hydrophobicity is inspired from the rose-petal effect or the gecko's feet [37-39]. This type of surfaces is characterized by a high water contact angle (exceeding  $150^\circ$ ) and a high water adhesion demonstrated by the firm pinning behavior of the water droplet to the surface at any sliding angle [40].

The wettability of surfaces plays an important role in different applications, and the creation of low water-adhesion super-hydrophobic coatings have attracted special interest due to their potential application for ultra-dry surfaces, self-cleaning and anti-fogging coatings. On the other hand, the high adhesive rose-petal super-hydrophobicity can be used in applications such as liquid transportation [41, 42] and single molecule spectroscopy [43].

The design of superhydrophobic surfaces based on ZnO nanorod arrays needs a combination of both rough hierarchical structures as well as low surface energy [44, 45]. Previous research consisted on the formation of superhydrophobic hierarchical micro-nano structures, by surface modification process using low surface free energy top-coatings [46, 47]. Xue et al. [48] fabricated superhydrophobic surfaces using ZnO nanorod arrays top-coated with Cu<sub>2</sub>O nanoparticles, which have a lower surface free energy compared to ZnO, and reported a static contact angle of 126° for the as-prepared ZnO nanorods compared to a maximum static angle of 166° after the deposition of Cu<sub>2</sub>O top coating. Also, in order to decrease the contact area between the water droplet and the material's surface, Zhu et al. [49] reports the fabrication of ZnO nanorod arrays followed by a surface modification with n-octadecanoic acid, exhibiting a contact angle of 159°. Likewise, Gyra et al. [50] and He et al. [51] fabricated ZnO nanorod arrays by a post-hydrophobization process using low surface energy provided by stearic acid (CA = 152°) and by surface fluorination (CA = 167°), respectively. Other research have been dedicated to study the effect of sticky super-hydrophobicity, or super-hydrophobicity with high sliding angles, due to high water adhesion using ZnO nanorods [34, 49, 52].

This present work consists on the fabrication of superhydrophobic ZnO surfaces based on dual-scale hierarchical structure based on the same material (ZnO top coated with ZnO). This is different from other research in the literature, which report the design of superhydrophobic ZnO nanorod arrays using post-hydrophobization treatment using different materials with low surface energy. The surface morphology, structure, wetting properties and switching behavior under UV light exposure, as well as the photo-catalysis ability of both hydrophobic single roughness surface, fabricated with ZnO nanorod arrays only, and super-hydrophobic dual roughness surface fabricated with ZnO nanorod arrays top coated with a layer of sputtered ZnO.

## 2. Experimental Details

### 2.1. Preparation of ZnO Nano rods

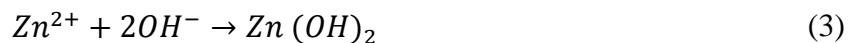
In this work, ZnO nanorod arrays (NRA) have been prepared by means of electrochemical deposition. The ZnO NRA are grown on 5x5 cm<sup>2</sup> fluorine doped tin oxide coated glass (FTO) substrates of 7 Ω/sq from Solaronix. Before the deposition, the FTO substrates were ultrasonically cleaned by successive rinsing in acetone, ethanol and ultra-pure H<sub>2</sub>O, after the substrates were cleaned, they were subsequently blown with Nitrogen to dry.

The ZnO NRA are electrochemically grown on top of the FTO substrate using a galvanostatic seeding step prior to potentiostatic growth [53]. Previous work by Canava and Lincot [54] demonstrates that an electrochemical activation step can be used to increase the nanowire density of electrodeposited ZnO nanowire arrays. Therefore, the galvanostatic seed layer is used to control the number of nucleation sites for ZnO NR growth [53].

The ZnO nanorod arrays prepared in this work were grown on the FTO substrates from a magnetically stirred aqueous solution of 5 mM of zinc nitrate [Zn(NO<sub>3</sub>)<sub>2</sub>·6H<sub>2</sub>O] and 5 mM of ammonium nitrate [NH<sub>4</sub>NO<sub>3</sub>] kept at a low temperature of 75 °C following the standard conditions presented by Riedel et al. [53].

The experimental set up is comprised of a three electrode system, with the substrate as the working electrode, a Platinum sheet as the counter electrode, and a Platinum wire as the pseudo reference electrode (potential remains during the deposition, -0.338V vs. Ag/AgCl). The ZnO nanorod array growth was started with a 40 s galvanostatic step applying a current density of 0.4 mA/cm<sup>2</sup>. The potentiostatic growth was subsequently conducted for 2000 s at a constant potential of -1.4 V vs. Pt.

The ZnO nanorod arrays are formed in nitrate based solutions following the reaction mechanism suggested by Izaki et al. [56-58]:





After the deposition, the prepared substrates were rinsed in water to remove residual salts and dried in nitrogen. Prior to further analysis, the samples were ultrasonically cleaned in Ethanol for 3 minutes, followed by pure water for 3 minutes, and then dried with Nitrogen to remove residual salts. The morphology of the ZnO NRA was observed using scanning electron microscopy (SEM).

## 2.2. Preparation of ZnO thin film using reactive magnetron sputtering

Intrinsic ZnO thin films were grown by mean of radio frequency magnetron sputtering on top of the ZnO nanorod arrays. The films were grown in pure Ar/O<sub>2</sub> atmosphere, with a power of 1.5 kW and a target-to-substrate distance of approx. 70 mm. The average deposition time for the intrinsic ZnO thin films was 10 min.

## 2.3. Photo-catalysis Test

The photo-catalysis of the ZnO nanorod arrays as well as the ZnO nanorods covered with sputtered ZnO (dual roughness) was evaluated using methylene blue hydrate (MB, C<sub>16</sub>H<sub>18</sub>ClN<sub>3</sub>S.xH<sub>2</sub>O, Fluka Analytical). The photo-degradation test was conducted using 20 ml of methylene blue solution with an initial concentration of 0.01 mMol/L in the presence of FTO substrates (25\*25\*2 mm) coated with ZnO nanorod arrays and ZnO double structured layers. The pH value of the prepared MB solution (pH = 6.8) was measured with an SP70P/VWR pH measurement instrument.

The concentration of the MB solution was calculated from the UV-Vis measurements of the absorption spectrum using an Avantes Ava Light-DH-S-BAL spectrophotometer. 700 µL of the solution was withdrawn each time interval and its optical absorption was measured.

In order to ensure that the dye degradation is due to the UV light exposure, and not on the absorption of the dye by the surface of the ZnO films, a dark test was first conducted by adding the ZnO single roughness and dual roughness films to the MB dye solution, and storing in the dark for 1 hour. The optical absorption of the dye after the dark test was taken as a baseline for the photo-catalysis test under UV illumination.

The photo-degradation test was conducted during a time interval ranging from 1 h to 5 h, the irradiation was provided by 2\*15 W UV lamps (NU-15 KL) with a radiation power of 2 mW/cm<sup>2</sup> and major emission at 365 nm. The MB solution was magnetically stirred during the experiment, with a rotation of 115 rpm.

The degradation of the MB dye was calculated from the absorption intensity reduction at wavelength ( $\lambda_{max} = 665 \text{ nm}$ ). The degradation efficiency (DE) was calculated using the Eq. (5):

$$DE (\%) = \frac{I_0 - I}{I_0} * 100 = \frac{C_0 - C}{C_0} * 100 \quad (5)$$

Where:

- $I_0$ : Initial absorption intensity of the MB dye at  $\lambda_{max} = 665 \text{ nm}$
- $I$ : Absorption intensity of the MB dye at  $\lambda_{max} = 665 \text{ nm}$  after photo-irradiation
- $C_0$ : Initial concentration of the dye ( $C_0 = 0.01 \text{ mMol/l}$ )
- $C$ : Concentration of the dye after photo-irradiation

In order to calculate the degradation efficiency, a knowledge of the concentration of the MB dye after photo-irradiation is needed. For this reason, the MB calibration curve was developed by preparing different MB solutions with different concentrations (0.001 mMol/l, 0.002 mMol/l, 0.003 mMol/l, 0.004 mMol/l, 0.005 mMol/l, 0.006 mMol/l, 0.007 mMol/l, 0.008 mMol/l, 0.009 mMol/l and 0.01 mMol/l), and their respective absorption spectra were measured.

## 2.4. Film Characterization

The crystalline structure of ZnO layers was determined by an X-ray diffractometer (Siemens D5000 XRD unit) in  $2\theta$  range from 20° to 80° by 0.07° s<sup>-1</sup> steps operating at 40 KV accelerating voltage and 40 mA current using CuK $\alpha$  radiation source with  $\lambda = 1.5406 \text{ \AA}$ .

The morphological investigations of the prepared films were achieved with a high-resolution Ultra 55 Zeiss FEG scanning electron microscope (FEGSEM) operating at an acceleration voltage of 10 kV.

The film thickness was determined using a Dektak8stylus profiler (stylus diamond tip radius = 12.5  $\mu\text{m}$ , vertical range from 5 nm to 1 mm, stylus tracking force range from 0.03 to 15 mg).



The optical properties of the prepared ZnO films were investigated by measuring the transmittance (T) and reflectance (R) using a UV-VIS-NIR Perkin Elmer Lambda 950 spectrophotometer, equipped with a 150 mm integrating sphere in the wavelength range from 200 nm to 2500 nm with a step width of 2nm. The absorbance (A) of the samples was estimated by  $A=100-T-R$ . Average values of T, R and A were calculated in the wavelength range from 250 nm to 2500 nm.

The wettability of the samples was evaluated using an OCA 15 plus contact angle system (micro-syringe with a droplet size of 5  $\mu$ l). The water drops' images were snapped 5 seconds after the deposition of the drop on the samples.

### 3. Results and Discussion

#### 3.1. Surface Structure of ZnO nanorod arrays

Figure 1 shows the FESEM top images of the ZnO nanorod arrays deposited on FTO. It can be seen that the substrate is covered with a uniform and dense ZnO nanorod arrays, possessing a rod-like structure with a hexagonal cross section. As illustrated in Figure 1 (a) and (b), the nanorod arrays have an average length of 710 nm, and an average width (diameter) of 156 nm. The as-prepared ZnO nanorod arrays show a hydrophobic behavior without any chemical modification, exhibiting a static water contact angle of 108°.

As depicted in Figure 1 (c, d), the XRD pattern shows the formation of the ZnO wurtzite hexagonal phase, which is dominated by the (002) crystallographic plane, confirming the strong (002) orientation of the ZnO phase, showing that ZnO grows along the c-axis direction, due to the lower surface energy and thermal stability of ZnO (0001) face. For the ZnO nanorod array top coated with sputtered ZnO (deposited on FTO substrate), the diffraction peaks located at  $2\theta = 31.7^\circ, 34.4^\circ, 36.2^\circ, 47.5^\circ, 56.6^\circ, 62.8^\circ, 67.9^\circ, 69.09^\circ$  and  $72.5^\circ$ , which correspond to the (100), (002), (101), (102), (110), (103), (112), (201) and (004) planes of the hexagonal wurtzite phase of zinc oxide, respectively. On the other hand, for the sputtered ZnO layer with a thickness of 100 nm deposited on a glass substrate, the diffraction peaks located at  $2\theta = 34.4^\circ, 36.2^\circ, 47.5^\circ$  and  $62.8^\circ$ , corresponding to the (002), (101), (102) and (103) crystallographic planes, were observed.

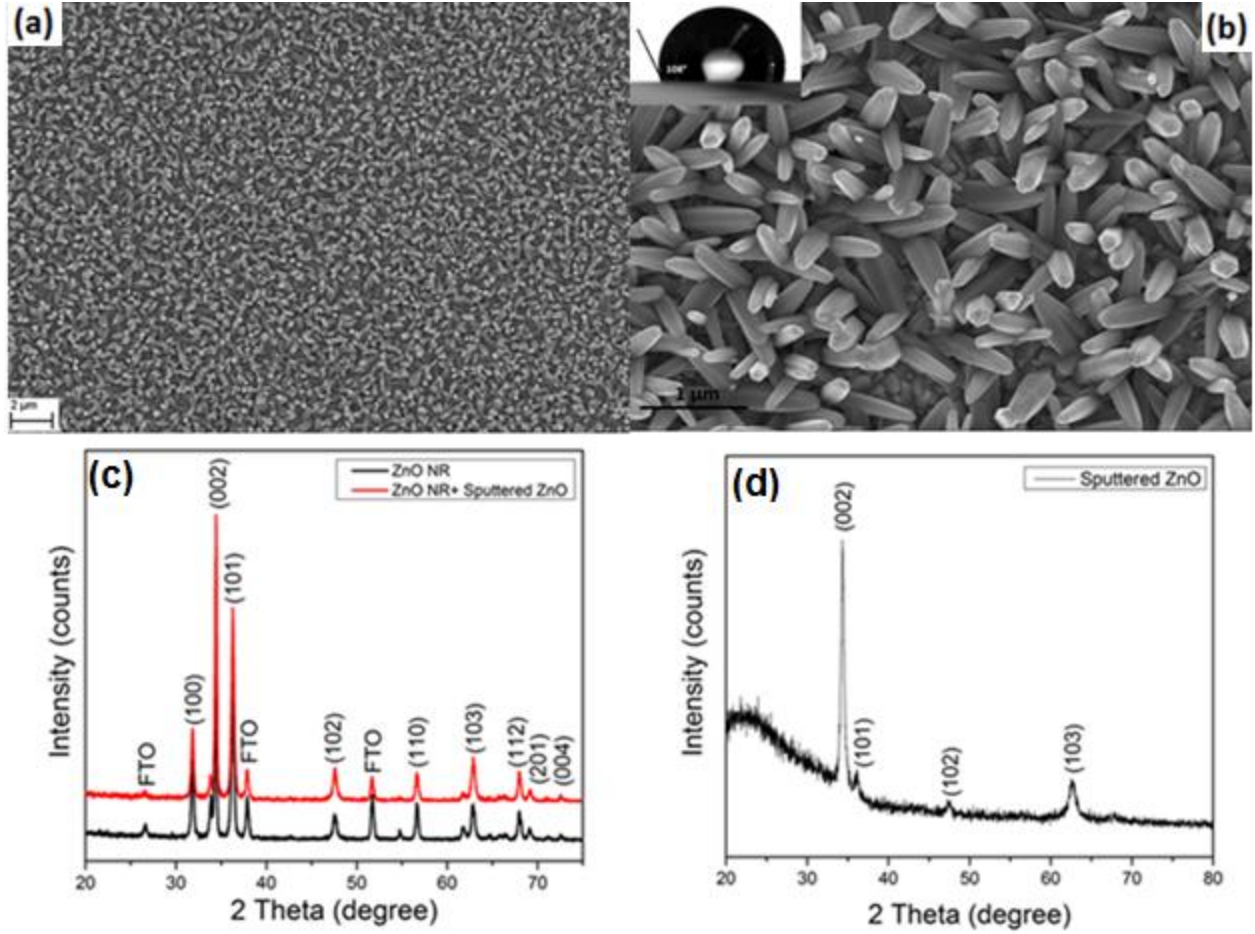


Figure 1. FESEM top images of the as-prepared ZnO nanorod at (a) low magnification and (b) high magnification (inset: water contact angle measurement on the single roughness ZnO nanorods); X-Ray Diffraction Pattern for (c) single roughness ZnO NRA and dual roughness ZnO NRA coated with sputtered ZnO (d) Sputtered ZnO layer with 100 nm thickness deposited on glass.

The crystallite size was estimated from the XRD data using the Debye-Scherrer equation [59, 60]:

$$d_{RX} = \frac{K\lambda}{\beta(2\theta) \cos \theta} \quad (6)$$

Where  $d_{RX}$  is the crystallite size,  $K$  is the Scherrer correlation constant to account for particle size ( $K = 0.9$ ),  $\lambda = 1.54 \text{ \AA}$  is the wavelength ( $Cu K\alpha$ ),  $\beta(2\theta)$  is the Full Width Half Maximum (FWHM) of the most intense peak (in radians) and  $\theta$  is the angle between the incident ray and the scattering planes (Bragg angle). The value of  $K$  was taken as 0.9 for Full Width Half Maximum (FWHM) of spherical crystals with cubic symmetry. Discussion of the values of  $K$  are available in the work of Langford et al. (1987) [61].

The estimated crystallite size of sputtered intrinsic ZnO deposited on glass from the XRD dominating peak corresponding to the crystallographic plane (002) is of 30 nm.

As shown in Figure 2, the grain size of sputtered ZnO film with a thickness of 100 nm deposited on silver-coated glass is 152 nm (Fig.2 (a)). The same ZnO sputtered layer has been deposited on top of FTO substrates, showing a crystallite size is of 30 nm (Fig.2 (b)), this result confirms the calculations conducted from the XRD pattern using the Debye-Scherrer equation.

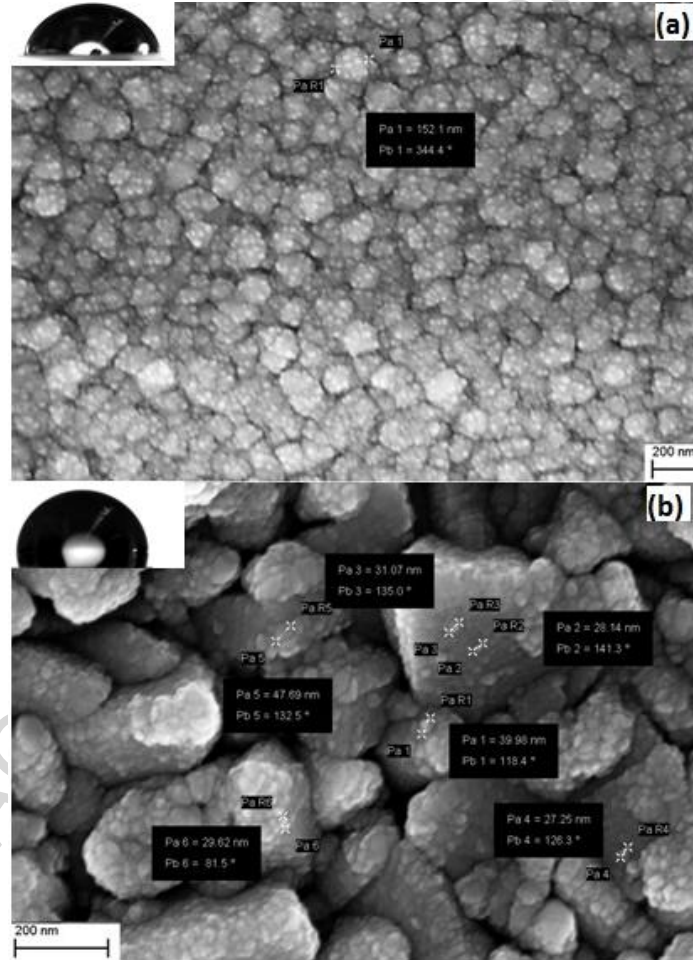


Figure 2. SEM of Sputtered ZnO (a) on Silver-coated glass substrate (b) on FTO substrate.

The as-deposited ZnO nanorod arrays exhibited a hydrophobic behavior, with a surface water contact angle of 108°. On the other hand, and as illustrated in Figure 3(b), the water contact angle measured on the surface of the single roughness ZnO nanorod arrays (108°) increases to 157° by the creation of a double structured ZnO layer, exhibiting a super-hydrophobic behavior.

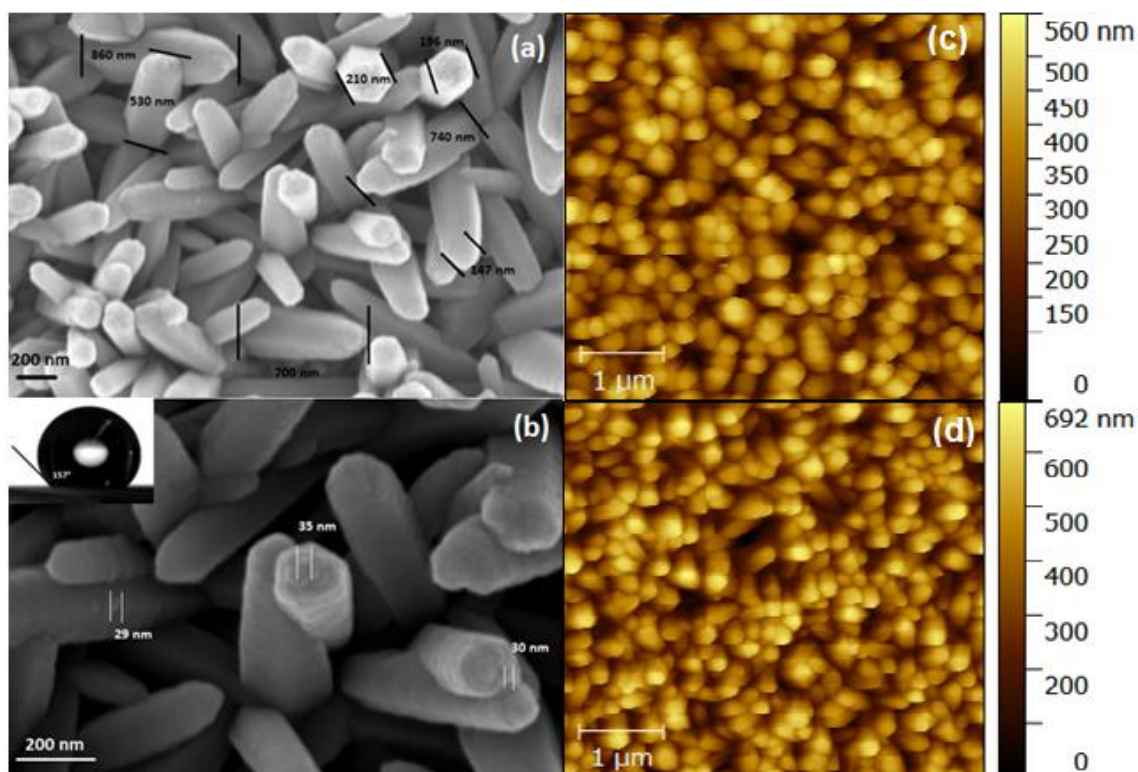


Figure 3. Scanning electron micrographs of the dual-roughness structured ZnO film (a) nanorod length and diameter (b) nanostructures on top of the ZnO nanorods (inset: water contact angle measurement on the double structured ZnO layer), AFM images of (c) single-roughness ZnO film and (d) dual-roughness structured ZnO film

As observed from Figure 3(b), small crystallites of 30 nm diameter are deposited on top and on the walls of the nanorods after ZnO sputtering. Also, the deposition of the sputtered ZnO top coating on top of the nanorods resulted in an increase in the surface roughness from 98 nm to 123 nm. In order to evaluate the wetting behavior of surfaces, a knowledge of the roll-off angle is of major importance. In fact, the Wenzel state is dominant for surfaces with sliding angle higher than  $20^\circ$  whereas the Cassie-Baxter state is dominant for surfaces with sliding angles lower than  $10^\circ$ . In this work, the hydrophobicity of the ZnO nanorod arrays was improved from  $108^\circ$  to  $157^\circ$  by creating a dual-roughness structure as depicted in Figure 3(b). The improvement of the water contact angle of the dual-roughness structured ZnO film compared to the as-deposited ZnO nanorod arrays is attributed to the increase in the surface roughness, making it favorable for a subsequent superhydrophobic behavior.

Considering the high enough packing density of the ZnO nanorod arrays and the low surface energy for the hydrophobic sputtered ZnO, it is possible to keep water droplets on top of the surface of ZnO nanorod arrays. This would result in a three-phase (air–water–solid interface) of

a water droplet, which leads to a higher contact angle. When the water droplet was suspended on top of the ZnO dual-roughness film, air would be trapped beneath it, following the Cassie regime expressed by Eq. (7), where ( $\theta_C$ ) is the apparent contact angle, ( $\phi_S$ ) and ( $\phi_V$ ) are the fractions of solid and air in contact with the water droplet ( $\phi_S + \phi_V = 1$ ), and ( $\theta_{LV}$ ) is the contact angle of water in air ( $\theta_{LV} = 180^\circ$ ):

$$\cos \theta_C = \phi_S \cos \theta_{Smooth} + \phi_V \cos \theta_{LV} = \phi_S \cos \theta_{Smooth} - (1 - \phi_S) \quad (7)$$

In the Cassie state, a decrease in the solid fraction contacting the water droplet ( $\phi_S$ ) would increase the apparent super-hydrophobicity of the surface, consequently, when more air is trapped in the surface asperities results in an increase in the apparent surface hydrophobicity.

Moreover, the wettability measurements show that both the prepared single-scale roughness ZnO nanorod arrays as well as the dual-scale ZnO NRA coated with sputtered ZnO are highly adhesive, with a very firm pinning behavior. In fact, the water droplet does not slide even with a vertical sliding angle, and even when the substrate is turned upside down, which is very similar to the rose-petal effect, resulting from the Cassie-impregnating sticky-type super-hydrophobic state. This result is in accordance with previous research, which shows that a rose-petal effect can be obtained by both single-scale and dual-scale roughness [62].

### 3.1. Optical Measurements

The optical transmittance of the deposited ZnO nanorod arrays (NRA), and ZnO nanorod arrays top-coated with sputtered ZnO was measured, showing that the layers were transparent in the visible range, with approximately 60 % transmittance for ZnO nanorod arrays deposited on FTO substrates (Fig.4 (b)), with a slight decrease of 2% after the deposition of the sputtered ZnO top coating layer.



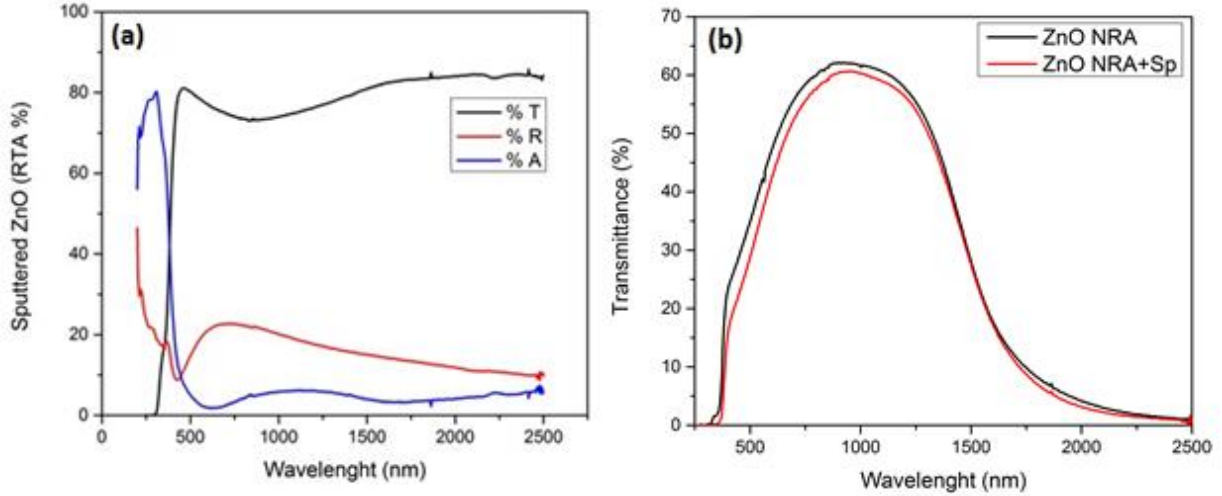
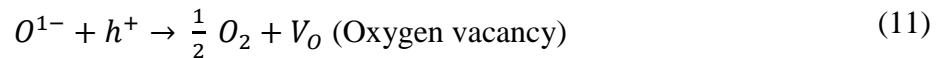
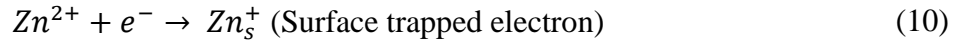
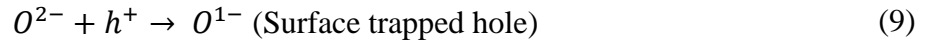


Figure 4. Optical measurements of (a) the sputtered ZnO deposited on glass (b) the as-grown ZnO NRA and the ZnO NRA coated with sputtered ZnO deposited on FTO.

### 3.1. Wetting Behavior under UV Illumination

The wettability of both samples was also studied under UV illumination. Previous research was dedicated to investigate the ZnO switching behavior from hydrophobicity to under UV light exposition [63, 64]. In fact, the illumination of ZnO layers with UV light with photon energy equal or higher than the band gap of ZnO (3.37 eV) generates electron-hole pairs in the surface of the ZnO layers. The electrons ( $e^-$ ) in the valence band are excited to the conduction band, and the same number of holes ( $h^+$ ) are generated in the valence band. The process that leads to the surface composition change is explained as follows:



Surface oxygen vacancies ( $\text{O}^{1-}$ ) are formed when some of the holes react with lattice oxygen ( $\text{O}^{2-}$ ), while defective ( $\text{Zn}_s^+$ ) sites are formed when some of the electrons react with the lattice metal ion ( $\text{Zn}^{2+}$ ). When the ZnO layers are in contact with water, the water molecules may adsorb at the oxygen vacancy ( $\text{V}_\text{O}$ ) site. The defective sites are kinetically more favorable for hydroxyl groups ( $\text{OH}^-$ ) adsorption than oxygen adsorption. Therefore, it stimulates increased water adsorption at the UV light irradiated ZnO layers, which results in a hydrophilic behavior of

the surface.  $\text{H}_2\text{O}$  and  $\text{O}_2$  can both adsorb on these defective sites. The surface trapped electrons ( $\text{Zn}_s^+$ ) tend to react with oxygen molecules adsorbed on the surface:



Light induced super-hydrophilicity was studied by irradiating both ZnO films using a Xenon lamp from Müller Elektronik-Optik with a power of 1400 W. After irradiating the samples for a 30 min interval, a 5  $\mu\text{l}$  droplet was placed in the irradiated samples, and the water contact angle was measured using the OCA 15 plus contact angle system.

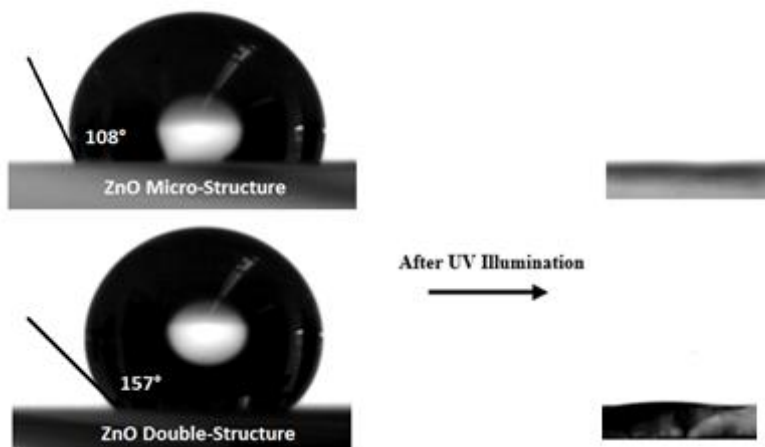


Figure 5. Water contact angle on the single roughness ZnO NRA and dual roughness structured ZnO NRA coated with sputtered ZnO before (left side) and after UV illumination (right side).

The water contact angle of both the ZnO single-scale and dual-scale roughness films decreased significantly after exposure to UV light, exhibiting a super-hydrophilic behavior, with a water contact angle of 0° and 5°, respectively after 30 minutes of UV exposure. The wetting behavior of both ZnO layer structures under UV illumination is shown in Figure 6.

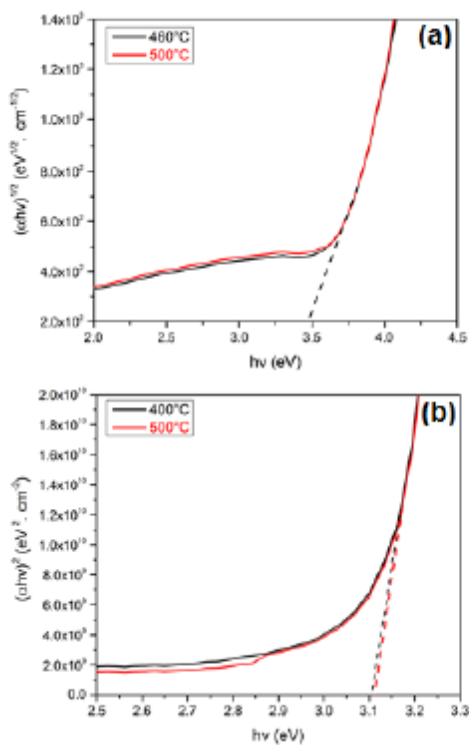


Figure 6. Plot of  $(\alpha h\nu)^{1/2}$  vs.  $h\nu$  for (a) TiO<sub>2</sub> indirect transition (b) for ZnO direct transition.  $E_g$  is obtained by extrapolating to  $(\alpha=0)$ .

### 3.2. Photo-catalysis Test

For the as-grown ZnO nanorod arrays, the photo-degradation of MB solution was of 50% after 5 h of UV exposition as illustrated in Figure 7 (a).



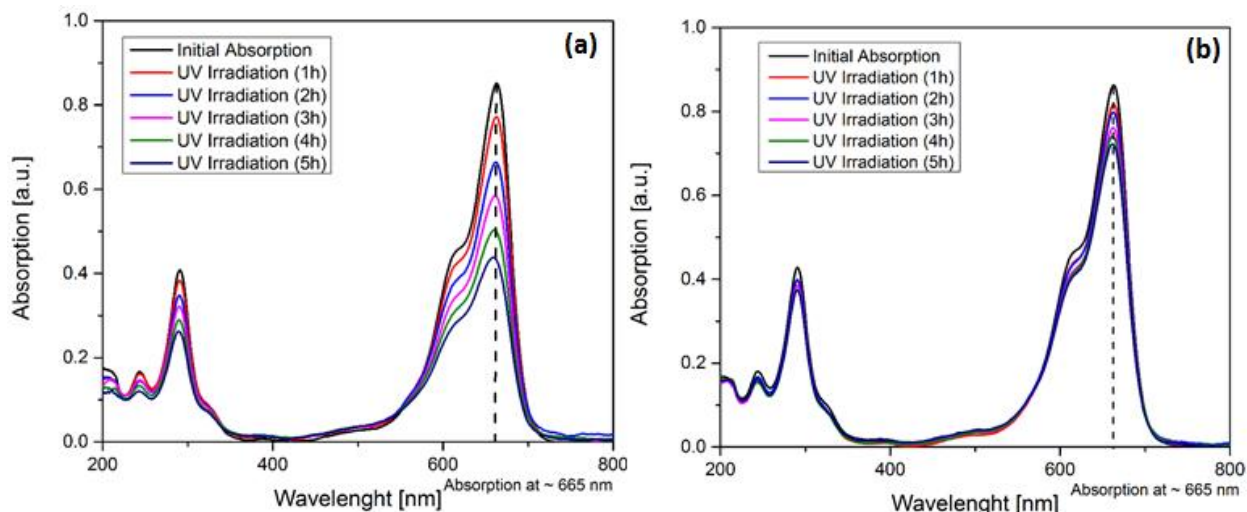


Figure 7. MB degradation by the photo-catalysis of (a) ZnO NRA (b) ZnO NRA top coated with sputtered ZnO

On the other hand, the photo-degradation decreased to 16%, for the ZnO nanorod arrays covered with a layer of sputtered ZnO (Fig. 7(b)), which is due to the super-hydrophobic behavior of the layer and the hydrophilic nature of the MB solution.

The results of the photo-catalysis test show that the degradation efficiency of the MB solution with ZnO nanorod arrays increased with the exposition time to UV light, with 9 % after 1 hour, 22 % after 2 hours, 31 % after 3 hours, 41 % after 4 hours and 50 % after 5 hours. On the other hand, the degradation test was conducted on the double-roughness ZnO film (ZnO NRA + sputtered ZnO). The results show a lower degradation efficiency of the MB solution. The degradation percent increased with the exposition time to UV light, with 5% after 1 hour, 7% after 2 hours, 12% after 3 hours, 14% after 4 hours and 16% after 5 hours.

The photo-degradation of the methylene blue solution can be fitted using Eq. (13), where the degradation constant  $k$  is obtained from the semi-logarithmic plot (plot of  $\ln(c/c_0)$  versus time) as illustrated in Figure 8 using the following equation [65]:

$$\ln\left(\frac{c}{c_0}\right) = -kt \quad (13)$$

After 5 hours of UV illumination, the ZnO nanorod arrays showed good activity, with a degradation efficiency of 50% and a degradation constant of ( $k = 0.00225 \text{ min}^{-1}$ ). On the other hand, the ZnO dual roughness structure prepared by sputtered ZnO on top of the ZnO nanorod

arrays showed minimal activity, with a degradation efficiency of 16% and a degradation constant of ( $k = 0.000586 \text{ min}^{-1}$ ) after 5 hours of UV exposure.

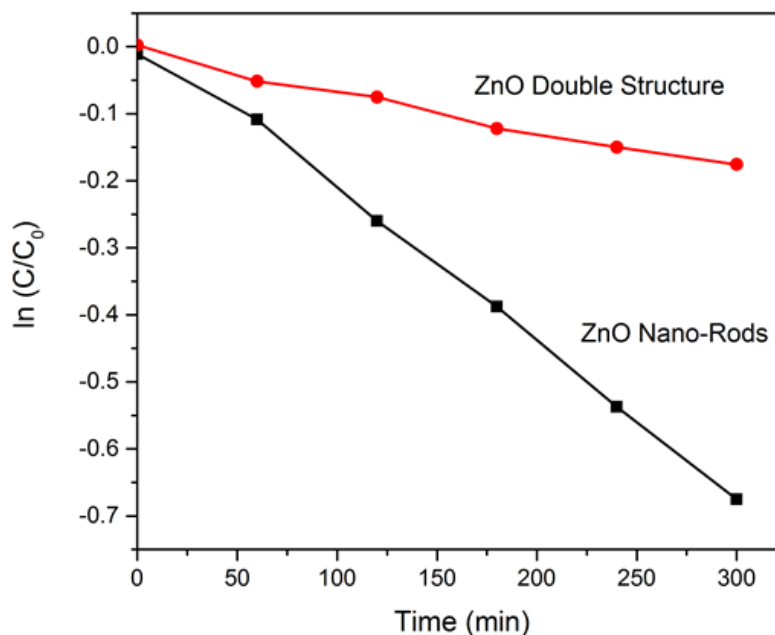


Figure 8. Photo-degradation of the methylene blue solution as a function of  $\ln (C/C_0)$  versus time of single roughness and dual roughness structured ZnO films.

The decrease in the photo-catalysis degradation of the dual-scale roughness ZnO NRA compared to the as-deposited ZnO NRA is due to the increase in the water contact angle ( $157^\circ$ ), which decreases the contact of the dye with the film, and therefore, leads to a lower photo-catalysis activity.

#### 4. Conclusion

In summary, super-hydrophobic surfaces based on structured ZnO nanorod arrays grown by means of low temperature electrochemical deposition were fabricated. The creation of a dual-scale roughness needed to achieve super-hydrophobicity is conducted by sputtering an intrinsic ZnO thin film with a crystallite size of 30 nm on top of the ZnO nanorod arrays, which leads to a water contact angle of  $157^\circ$ . The single-scale roughness ZnO NRA as well as the dual-scale ZnO NRA coated with sputtered ZnO showed very high water adhesion due to high van der Waals forces. In fact, the water droplet was firmly pinned to the film surface and did not slide even with tilt angles up to  $180^\circ$ , which is very similar to the rose-petal effect, known as the Cassie-

impregnating super-hydrophobic regime. Moreover, both prepared films exhibited high sensitivity to UV light, with a UV-induced switching behavior from super-hydrophobic to super-hydrophilic after only 30 minutes of UV exposure.

## Acknowledgments

This work has been done in the framework of the InnoTherm II project “Nano Coating and Testing: a step towards the improvement of CSP reflectors for less intensive maintenance both in terms of labor and water” supported by IRESEN (Institut de Recherche en Energie Solaire et Energies Nouvelles). The authors would also like to thank the DAAD, for financing the first author of this work.

## References

- [1] V. Srikant, D.R. Clarke, On the optical band gap of zinc oxide, *Journal of Applied Physics* 83(10) (1998) 5447-5451.
- [2] H. Chik, J. Liang, S.G. Cloutier, N. Kouklin, J.M. Xu, Periodic array of uniform ZnO nanorods by second-order self-assembly, *Applied Physics Letters* 84(17) (2004) 3376-3378.
- [3] I. Poulios, D. Makri, X. Prohaska, Photocatalytic treatment of olive milling waste water: oxidation of protocatechuic acid, *Global Nest: The International Journal* 1 (1999) 55-62.
- [4] S. Baruah, R.F. Rafique, J. Dutta, Visible light photocatalysis by tailoring crystal defects in zinc oxide nanostructures, *Nano* 3(5) (2008) 1-9.
- [5] A. C. Cakir, S. Erten-Ela, Comparison between synthesis techniques to obtain ZnO nanorods and its effect on dye sensitized solar cells, *Advance Powder Technology* 23(5) (2012) 655-660.
- [6] F. D. Nayeri, M. Kolahdouz, E. Asl-Soleimani, S. Mohajerzadeh, Low temperature carving of ZnO nanorods into nanotubes for dye-sensitized solar cell application, *Journal of Alloys and Compounds* 633 (2015) 359-365.
- [7] P. S. Kumar, J. Sundaramurthy, X. Zhang, D. Mangalaraj, V. Thavasi, S. Ramakrishna, Superhydrophobic and antireflecting behavior of densely packed and size controlled ZnO nanorods, *Journal of Alloys and Compounds* 553 (2013) 375-382.
- [8] J. Chen, H. Ye, L. Ae, Y. Tang, D. Kieven, T. Rissom, J. Neuendorf, M. Ch. Lux-Steiner, Tapered aluminum-doped vertical zinc oxide nanorod arrays as light coupling for solar energy applications, *Solar Energy Materials and Solar Cells* 95 (201) 1437-1440.

- [9] B.-K. Shin, T. Lee, J. Xiong, C. Hwang, G. Noh, J.-H. Cho, J.-M. Myoung, Bottom-up grown ZnO nanorods for an antireflective moth-eye structure on CuInGaSe<sub>2</sub> solar cells, *Solar Energy Materials and Solar Cells* 95(9) (2011) 2650-2654.
- [10] L. A  , J. Chen, M.Ch. Lux-Steiner, Hybrid flexible vertical nanoscale diodes prepared at low temperature in large area, *Nanotechnology* 19 (2008) 475201.
- [11] G. Wang, D. Chen, H. Zhang, J.Z. Zhang, J. Li, Tunable photocurrent in well-oriented zinc oxide nanorod arrays with enhanced photocatalytic activity, *Journal of Physical Chemistry C* 112 (2008) 8850-8855.
- [12] X. Yang, A. Wolcott, G. Wang, A. Sobo, R.C. Fitzmorris, F. Qian, J.Z. Zhang, Y. Li, Nitrogen-doped ZnO nanowire arrays for photoelectrochemical water splitting, *Nano Letters* 9(6) (2009) 2331-2336.
- [13] M. Fekete, W. Ludwig, S. Gledhill, J. Chen, A. Patti, L. Spiccia, Al-modified zinc oxide nanorods for photoelectrochemical water oxidation, *European Journal of Inorganic Chemistry* 4 (2014) 750-759.
- [14] B. S. Kang, Y. W. Heo, L. C. Tien, D. P. Norton, F. Ren, B.P. Gila, S .J. Pearton, Hydrogen and ozone gas sensing using multiple ZnO nanorods, *Applied Physics A* 80 (2005) 1029-1032.
- [15] J. X. Wang, X. W. Sun, Y. Yang, H. Huang, Y. C. Lee, O. K. Tan, L. Vayssieres, Hydrothermally grown oriented ZnO nanorod arrays for gas sensing applications, *Nanotechnology* 17 (2006) 4995.
- [16] Y. C. Kong, D. P. Yu, B. Zhang, W. Fang, S. Q. Feng, Ultraviolet-emitting ZnO nanowires synthesized by a physical vapor deposition approach, *Applied Physics Letters* 78(4) (2001) 407-409.
- [17] R. Teki, T .C. Parker, H. Li, N. Koratkar, T. M. Lu, S. Lee, Low temperature synthesis of single crystalline ZnO nanorods by oblique angle deposition, *Thin Solid Films*, 516(15) (2008) 4993-4996.
- [18] J.J. Wu, S.C. Liu, Low-temperature growth of well-aligned ZnO nanorods by chemical vapor deposition, *Advanced Materials* 14(3) (2002) 215-218.
- [19] B. Liu and H. C. Zeng, Hydrothermal synthesis of ZnO nanorods in the diameter regime of 50 nm, *Journal of the American Chemical Society* 125(15) (2003) 4430-4431.

- [20] Y. W. Heo, D. P. Norton, L. C. Tien, Y. Kwon, B. S. Kang, F. Ren, S. J. Pearton, J. R. LaRoche, ZnO nanowire growth and devices, *Materials Science of Engineering: R: Reports* 47(1-2) (2004) 1-47.
- [21] C. J. Chang, S. T. Hung, C. K. Lin, C. Y. Chen, E. H. Kuo, Selective growth of ZnO nanorods for gas sensors using ink-jet printing and hydrothermal processes, *Thin Solid Films* 519 (2010) 1693–1698.
- [22] R. Kitsomboonloha, S. Baruah, M. T. Z. Myint, V. Subramanian, J. Dutta, Selective growth of zinc oxide nanorods on inkjet printed seed patterns, *Journal of Crystal Growth* 311(8) (2009) 2352–2358.
- [23] L. Vayssieres, Growth of arrayed nanorods and nanowires of ZnO from aqueous solutions, *Advanced Materials* 15(5) (2003) 464-466.
- [24] Y. W. Wang, L. D. Zhang, G. Z. Wang, X. S. Peng, Z.Q. Chu, C.H. Liang, Catalytic growth of semiconducting zinc oxide nanowires and their photoluminescence properties, *Journal of Crystal Growth* 234(1) (2002) 171-175.
- [25] H. Z. Zhang, X. C. Sun, R. M. Wang, D. P. Yu, Growth and formation mechanism of c-oriented ZnO nanorod arrays deposited on glass, *Journal of Crystal Growth* 269(2-4) (2004) 464-471.
- [26] Y. Sun, G.M. Fuge, M.N.R. Ashfold, Growth mechanisms for ZnO nanorods formed by pulsed laser deposition, *Superlattices Microstructures* 39(1-4) (2006) 33-40.
- [27] Th. Pauporté, D. Lincot, Hydrogen Peroxide Oxygen Precursor for Zinc Oxide Electrodeposition I. Deposition in Perchlorate Medium, *Journal of the Electrochemical Society* 148(4) (2001) C310.
- [28] Th. Pauporté, D. Lincot, B. Viana, F. Pellé, Toward laser emission of epitaxial nanorod arrays of ZnO grown by electrodeposition, *Applied Physics Letters* 89 (2006) 233112.
- [29] W.J. Li, E.W. Shi, W.Z. Zhong, Z.W. Yin, Growth mechanism and growth habit of oxide crystals, *Journal of Crystal Growth* 203(1) (1999) 186–196.
- [30] E.R. Carraway, A.J. Hoffman, M.R. Hoffmann, Photocatalytic oxidation of organic acids on quantum-sized semiconductor colloids, *Environmental Science and Technology* 28 (1994) 786-793.
- [31] S. Herminghaus, Roughness-induced non-wetting, *Europhysics Letters* 52(2) (2000) 165–170.

- [32] M.T.Z. Myint, R. Kitsomboonloha, S. Baruah, J. Dutta, Superhydrophobic surfaces using selected zinc oxide microrod growth on ink-jetted patterns, *Journal of Colloid and Interface Science* 354 (2011) 810–815.
- [33] J. Li, Y. Yang, F. Zha, Z. Lei, Facile fabrication of superhydrophobic ZnO surfaces from high to low water adhesion, *Materials Letters* 75 (2012) 71-73.
- [34] C. Florica, N. Preda, M. Enculescu, I. Zgura, M. Socol, I. Enculescu, Superhydrophobic ZnO networks with high water adhesion, *Nanoscale Research Letters* 2014, 9:385.
- [35] J. Li, X. Liu, Y. Ye, J. Chen, Gecko-inspired synthesis of superhydrophobic ZnO surfaces with high water adhesion, *Colloids and Surfaces A: Physicochemical and Engineering aspects* 384(1-3) (2011) 109-114.
- [36] B. Bhushan, Biomimetics: lessons from nature-an overview, *Philosophical Transactions of the Royal Society A* 367 (2009) 1445-1486.
- [37] Y. A. Autumn, S. T. Liang, W. Hsieh, W. P. Zesch, T. W. Chan, R. Kenny, R. J. Fearing, Full, adhesive force of a single gecko foot-hair. *Nature* 405 (2000) 681-685.
- [38] B. Bhushan, E. K. Her, Fabrication of superhydrophobic surfaces with high and low adhesion inspired from rose petal, *Langmuir* 26(11) (2010) 8207-8217.
- [39] L. Feng, Y. Zhang, J. Xi, Y. Zhu, N. Wang, F. Xia, L. Jiang, Petal Effect: A Superhydrophobic State with High Adhesive Force, *Langmuir* 24(8) (2008) 4114-4119.
- [40] J. Li, X. Liu, Y. Ye, H. Zhou H, J. Chen, A facile solution-immersion process for the fabrication of superhydrophobic surfaces with high water adhesion, *Materials Letters* 66(1) (2012) 321-323.
- [41] M. Jin, X. Feng, L. Feng, T. Sun, J. Zhai, T. Li, L. Jiang, Superhydrophobic Aligned Polystyrene Nanotube Films with High Adhesive Force, *Advanced Materials* 17(16) (2005) 1977-1981.
- [42] X. Hong, X. Gao, L. Jiang, Application of superhydrophobic surface with high adhesive force in no lost transport of superparamagnetic microdroplet, *Journal of the American Society* 129 (2007) 1478-1479.
- [43] A. Winkleman, G. Gotesman, A. Yoffe, R. Naaman, Immobilizing a drop of water: fabricating highly hydrophobic surfaces that pin water droplets, *Nano Letters* 8(4) (2008) 1241-1245.

- [44] A. Shastry, M.J. Case, K.F. Bohringer, Directing droplets using microstructured surfaces, *Langmuir* 22(14) (2006) 6161-6167.
- [45] P. Joseph, C. Cottin-Bizonne, J.M. Benoît, C. Ybert, C. Journet, P. Tabeling, L. Bocquet, Slippage of Water Past Superhydrophobic Carbon Nanotube Forests in Microchannels, *Physical Review Letters* 97(15) (2006) 1-23.
- [46] X. Zhua, Z. Zhanga, X. Mena, J. Yanga, X. Xu, Fabrication of an intelligent superhydrophobic surface based on ZnO nanorod arrays with switchable adhesion property, *Applied Surface Science* 256 (2010) 7619-7622.
- [47] Y. Shi, W. Yang, X. Feng, Y. Wang, G. Yue, Fabrication of superhydrophobic ZnO nanorod surface with corrosion resistance via combining thermal oxidation and surface modification, *Materials Letters* 151(2015)24-27.
- [48] M. Xue, W. Wang, F. Wang, J. Ou, W. Li, Design and understanding of superhydrophobic ZnO nanorod arrays with controllable water adhesion, *Surface & Coatings Technology* 258 (2014) 200-205.
- [49] X. Zhua, Z. Zhang, X. Men, J. Yang, X. Xu, Fabrication of an intelligent superhydrophobic surface based on ZnO nanorod arrays with switchable adhesion property, *Applied Surface Science* 256 (2010) 7619-7622.
- [50] A. B. Gurav, S. S. Latthe, R. S. Vhatkar, J. G. Lee, D. Y. Kim, J. J. Park, S. S. Yoon, Superhydrophobic surface decorated with vertical ZnO nanorods modified by stearic acid, *Ceramics International* 40 (2014) 7151–7160.
- [51] G. He, K. Wang, The super hydrophobicity of ZnO nanorods fabricated by electrochemical deposition method, *Applied Surface Science* 257 (2011) 6590–6594.
- [52] M. T. Z. Myint, G. L. Hornyak, J. Dutta, One pot synthesis of opposing ‘rose petal’ and ‘lotus leaf’ superhydrophobic materials with zinc oxide nanorods, *Journal of Colloid and Interface Science* 415 (2014) 32-38.
- [53] B. Canava, D. Lincot, Nucleation effects on structural and optical properties of electrodeposited zinc oxide on tin oxide, *Journal of Applied Electrochemistry*. 30 (2000) 711.
- [54] W. Riedel, Y. Tang, W. Ohm, J. Chen, M. C. Lux-Steiner, S. Gledhill, Effect of initial galvanic nucleation on morphological and optical properties of ZnO nanorod arrays, *Thin Solid Films* 574 (2015) 177–183.

- [56] M. Izaki, T. Omi, Electrolyte Optimization for Cathodic Growth of Zinc Oxide Films, *Journal of the Electrochemical Society* 143(3) (1996) L53-55.
- [57] M. Izaki, T. Omi, Transparent Zinc Oxide Films Chemically Prepared from Aqueous Solution, *Journal of the Electrochemical Society* 144(1) (1997) L3-5.
- [58] M. Izaki, T. Omi, Transparent zinc oxide films prepared by electrochemical reaction, *Applied Physics Letters* 68(17) (1996) 2439-2440.
- [59] B. D. Cullity, *Elements of X-Ray Diffraction*, second ed., Addison Wesley, reading, MA, 1978.
- [60] P. Scherrer, Bestimmung der Grösse und der inneren Struktur von Kolloidteilchen mittels Röntgenstrahlen, *Nachr. Ges. Wiss. Göttingen, Mathematisch-Physikalische Klasse* 26 (1918) 98-100.
- [61] J.I. Langford and A.J.C. Wilson, Scherrer after Sixty Years: A Survey and Some New Results in the Determination of Crystallite Size, *Journal of Applied Crystallography* 11 (1978) 102-113.
- [62] K. Y. Yeh, K. H. Cho, Y. H. Yeh, A. Promraksa, C. H. Huang, C. C. Hsu, L. J. Chen, Observation of the rose petal effect over single- and dual-scale roughness surfaces, *Nanotechnology* 25 (2014) 345303.
- [63] V. Khranovskyy, T. Ekblad, R. Yakimova, L. Hultman, Surface morphology effects on the light-controlled wettability of ZnO nanostructures, *Applied Surface Science* 258 (2012) 8146.
- [64] L. Yao, M. Zheng, C. Li, L. Ma, W. Shen, Facile synthesis of superhydrophobic surface of ZnO nanoflakes: chemical coating and UV-induced wettability conversion, *Nanoscale Research Letters* 7:216 (2012).
- [65] Y.J. Li, X. D. Li, J. W. Li, J. Yin, Photocatalytic degradation of methyl orange by TiO<sub>2</sub>-coated activated carbon and kinetic study, *Water Research* 40(6) (2006) 1119-1126.